

Figure 1. Simplified geologic map showing the location of the Greater Green River Basin, the ERDA 1 Blacks Fork core (this study), and the Arco Oil and Gas WB-1 core (Carroll et al., 2008) (modified from Roehler, 1992; Smith et al., 2008; and Jagniecki et al., 2013).

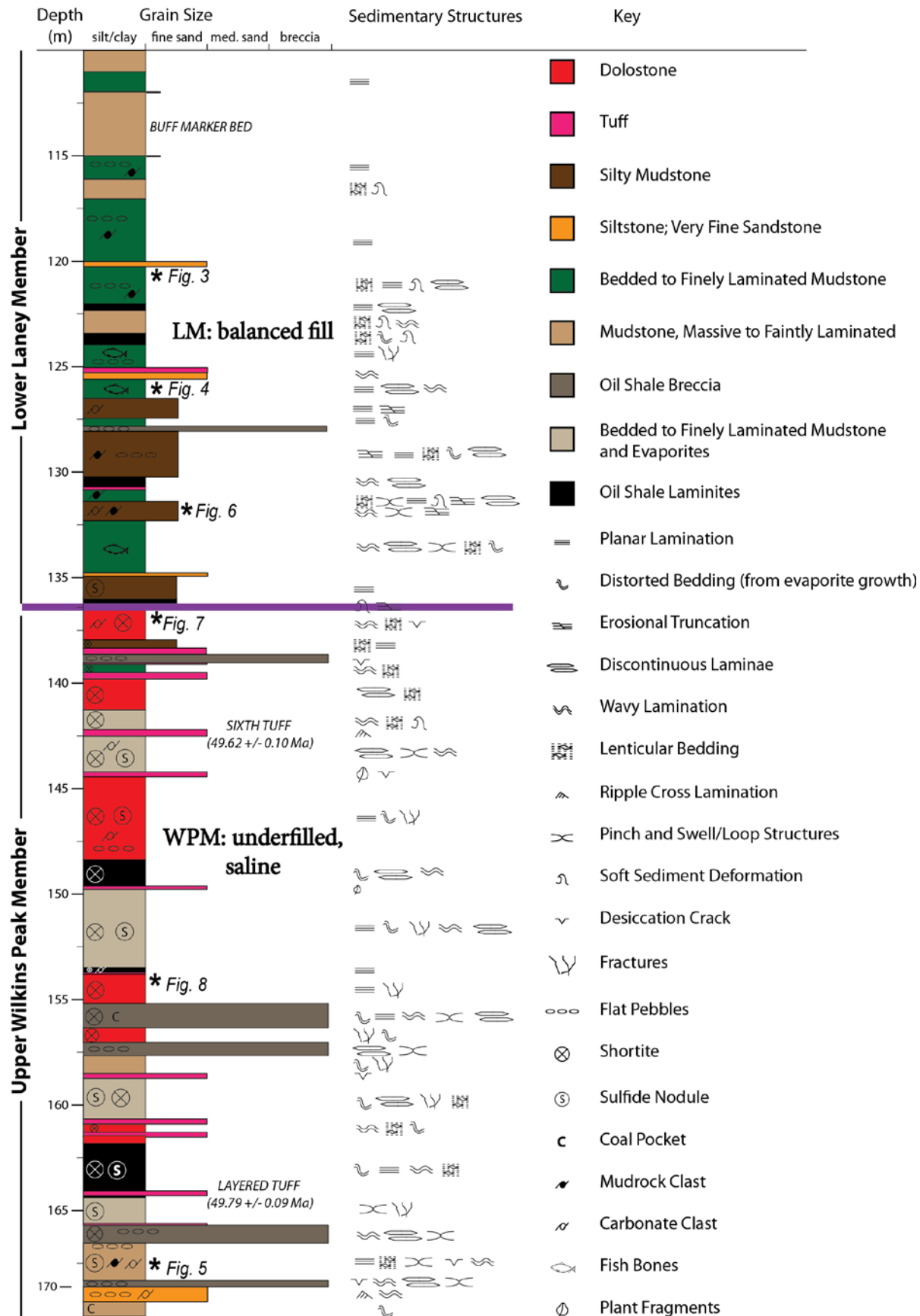


Figure 2. ERDA 1 Blacks Fork core from the Wilkins Peak Member-Laney Member transitional zone. The section shows a change from predominantly saline mudflat deposits in the WPM to perennial lacustrine deposits in the LM. Saline mudflat deposits from the WPM are poorly laminated, organic-poor carbonate mudstones, bedded to massive, that contain desiccation cracks, shortite, and sulfide minerals. Perennial lacustrine deposits are organic-rich, finely laminated couplets of carbonate and organic material.

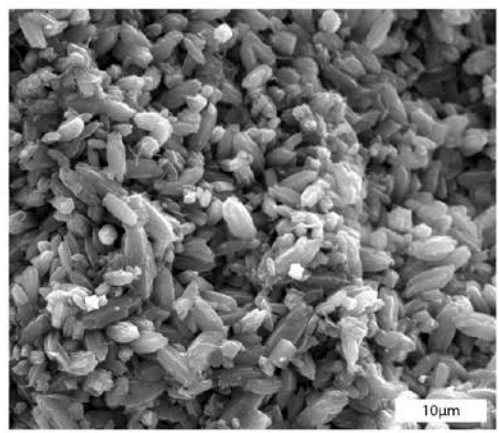
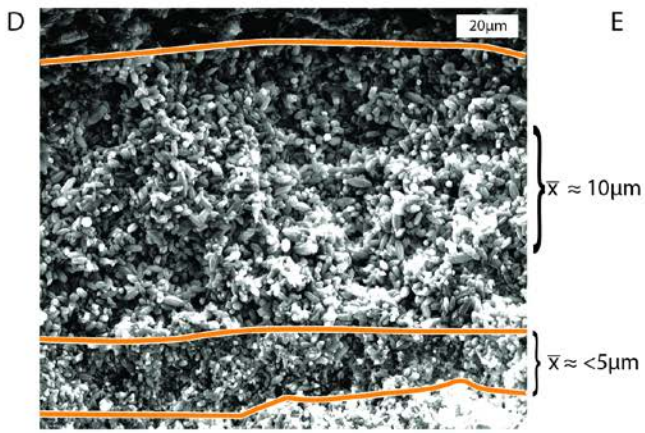
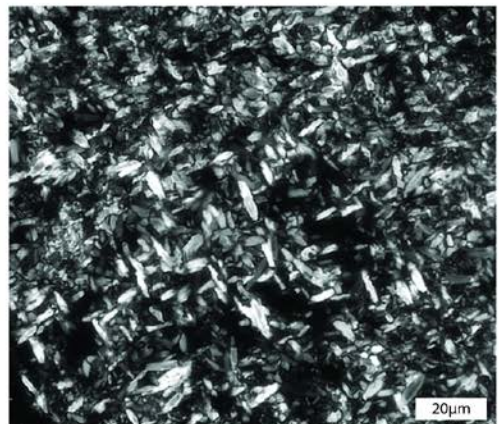
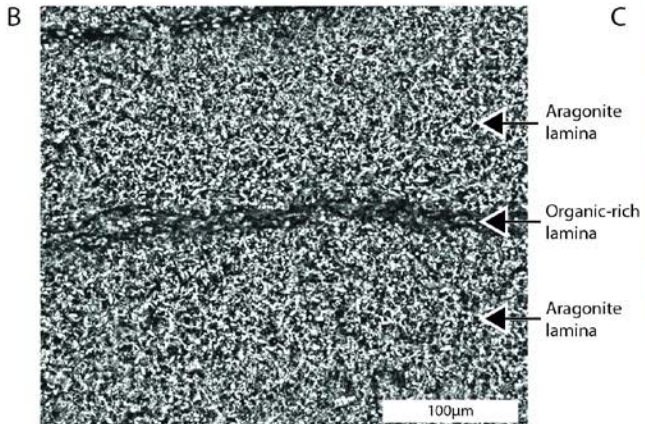
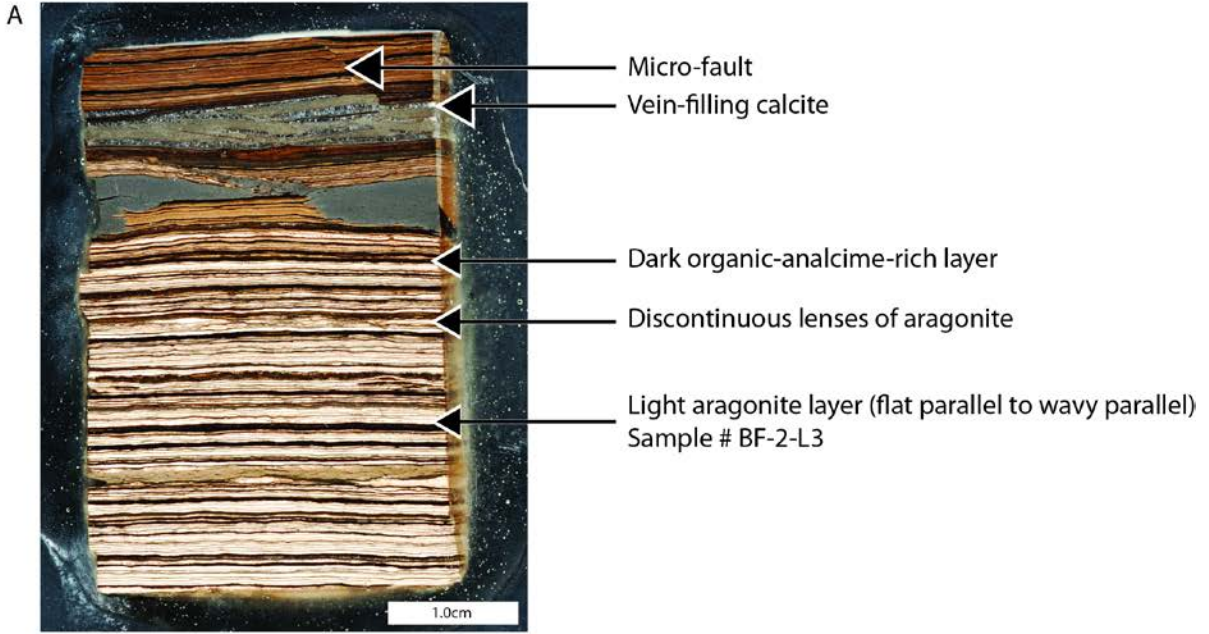


Figure 3. Hand sample (A), thin section (C), and SEM images (B,D,E) of aragonite laminae from the Laney Member sample JTM-BF-2, ERDA Blacks Fork 1 Core, 121.2m. A) Hand sample image showing 100 $\mu$ m scale lamination defined by light aragonite layers and dark organic-analcime-rich layers. Aragonite forms continuous laminae to discontinuous lenses; layering is flat parallel to wavy and crinkly. Micro-faults and vein-filling calcite occur in the upper portion of the sample. B) Backscatter SEM image showing laminae of unconsolidated aragonite illustrating random orientation of needle-shaped crystals. C) Thin section image of aragonite showing randomly oriented  $\sim$ 10 $\mu$ m diameter needles. D) SEM image of pure unconsolidated aragonite needles. Aragonite layer shows internal lamination defined by crystal size variation (the bottom portion is comprised of less than 5 $\mu$ m diameter crystals and upper sub-laminae with  $\sim$ 10 $\mu$ m diameter needles. E) SEM image of unconsolidated prismatic aragonite.

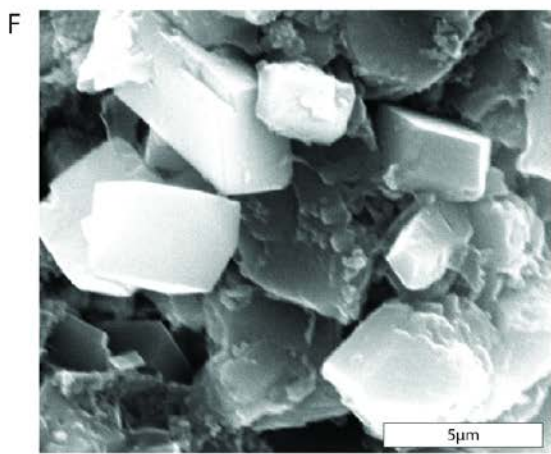
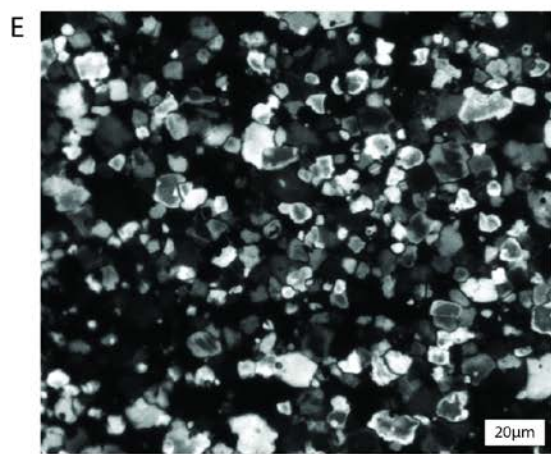
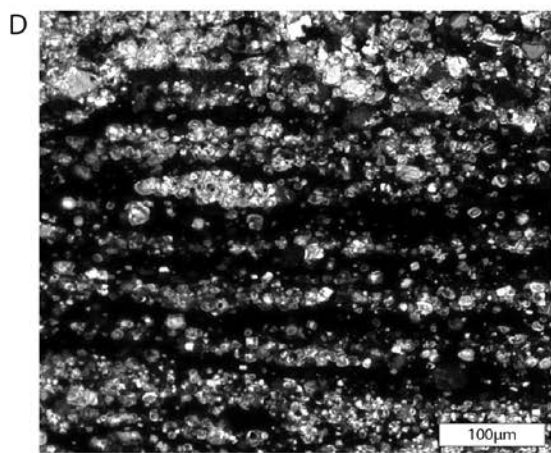
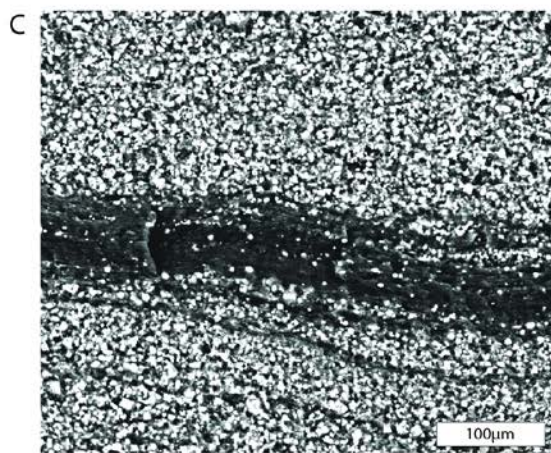
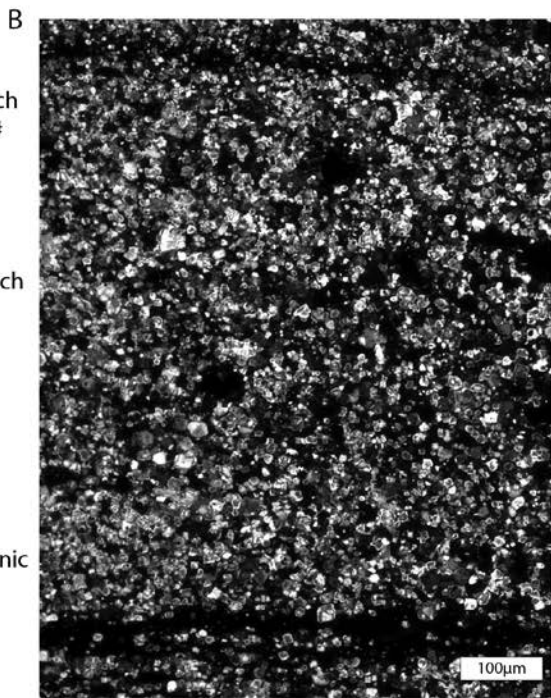
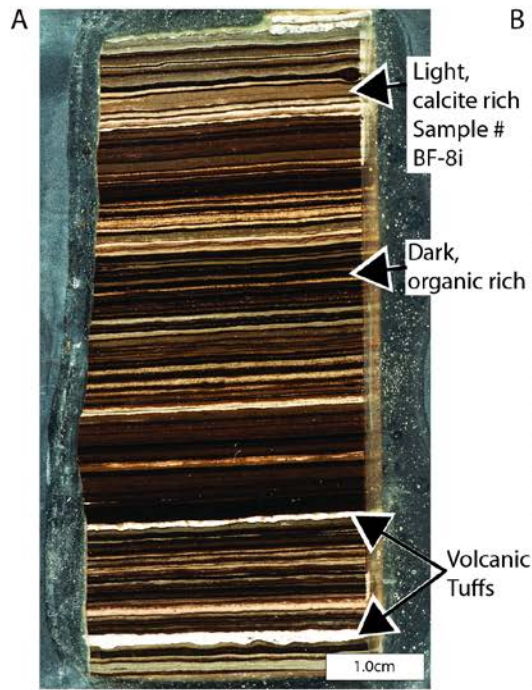


Figure 4. Hand sample (A), thin section (B, D, E), and SEM images (C, F) of primary precipitated calcite from the Laney Member, ERDA Blacks Fork 1 Core, JTM-BF-8, 125.9m. A) Hand sample image showing alternating light calcite and darker, organic-rich laminae. Pure calcite laminae are  $<50\mu\text{m}$  to  $800\mu\text{m}$  in thickness. Variable amounts of organic matter are mixed with calcite which influences color variations in individual laminae. Layering is flat to wavy and continuous across the width of the core. Two tuffaceous laminae occur near the bottom of this sample. B) Thin section image showing well sorted ( $\sim 10\mu\text{m}$  diameter crystals) calcite with dark patches of organic material. C) Backscatter SEM image of calcite crystal laminae and dark micro-laminated organic material. D) Thin-section image displaying thin layers of organic material which separate primary calcite laminae. Calcite crystals also occur within the organic layers. E) Thin section image of primary equant calcite crystals  $\sim 10\mu\text{m}$  in diameter in a layer with  $>90\%$  calcite and less than 10% dolomite and quartz. Amorphous dark areas are organic matter. F) SEM image of unconsolidated primary calcite crystals.

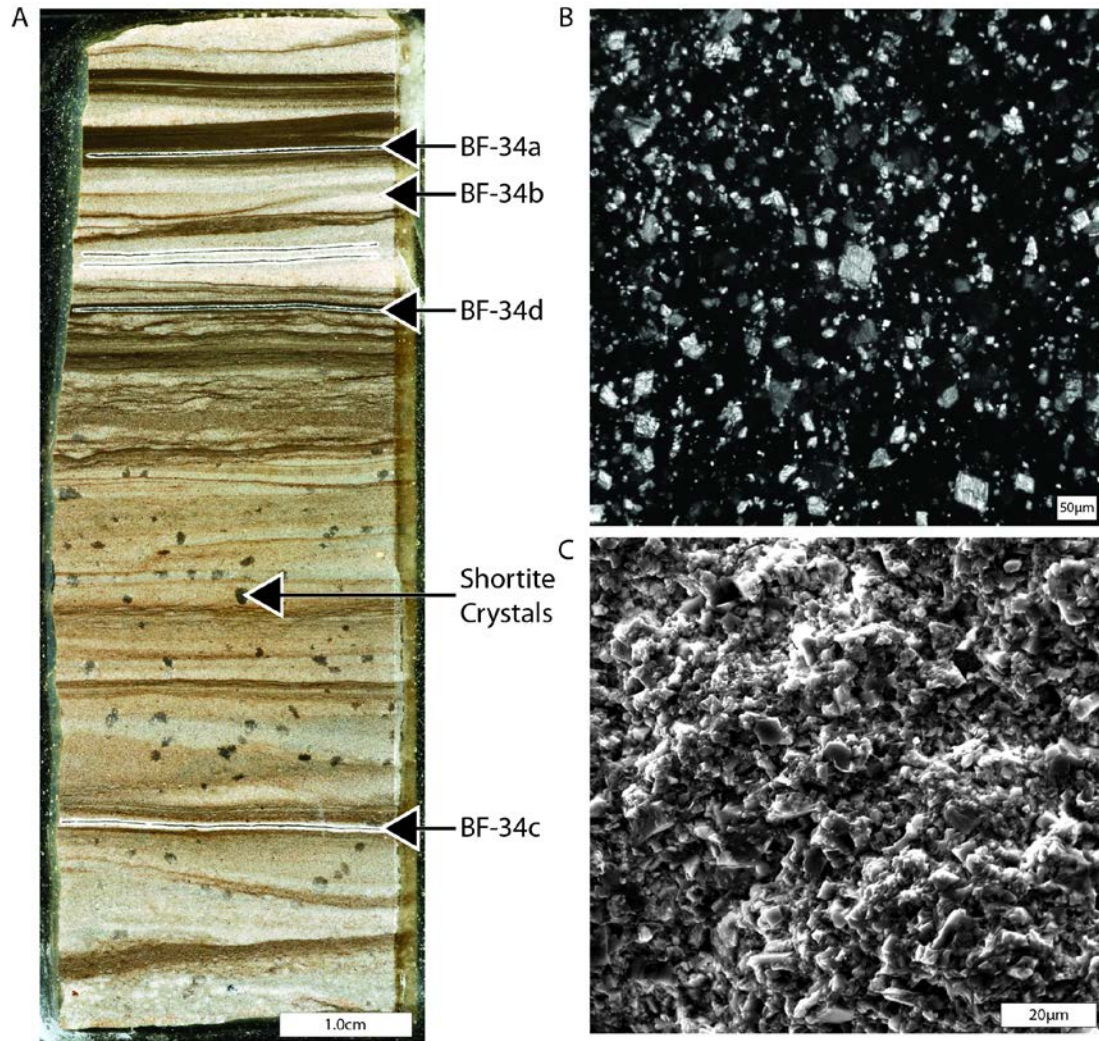


Figure 5. Hand sample (A), thin section (B) and SEM (C) image of primary dolomite from the Wilkins Peak Member, sample BF-34, 168.2m depth. A) Hand sample image of alternating coarser carbonate very fine sand (sample numbers BF-34b, BF-34c) and finer dolomite mud (BF-34a, BF-34d). Large crystals in the lower portion of the hand sample are shortite. B) Thin section image of laminae sample # BF-34a. Crystal sizes vary from  $<5\mu\text{m}$  to  $\sim 50\mu\text{m}$  in diameter with the majority finer than  $15\mu\text{m}$  in diameter. Finer crystals are subhedral to anhedral whereas coarser crystals are euhedral and terminate into primary pore space. C) SEM image of laminae sample

#BF-34a showing well-sorted, pure, unconsolidated crystals of dolomite. XRD analysis indicates that this lamina consists of 84% dolomite.

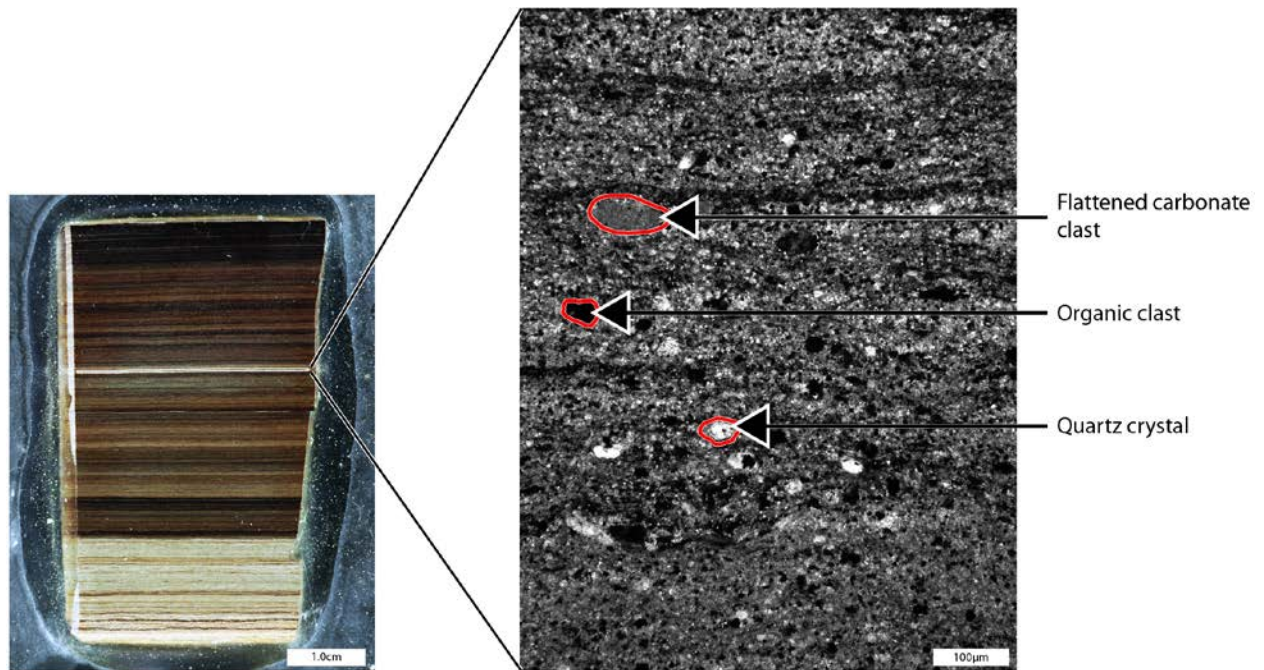
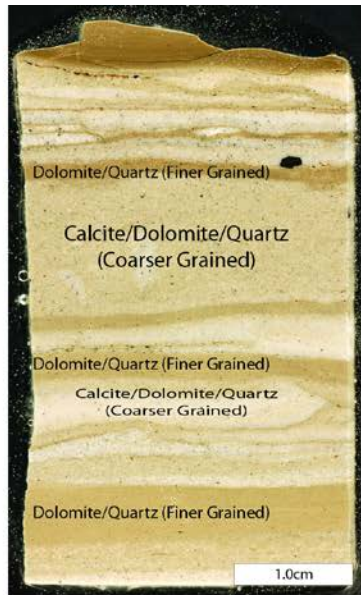
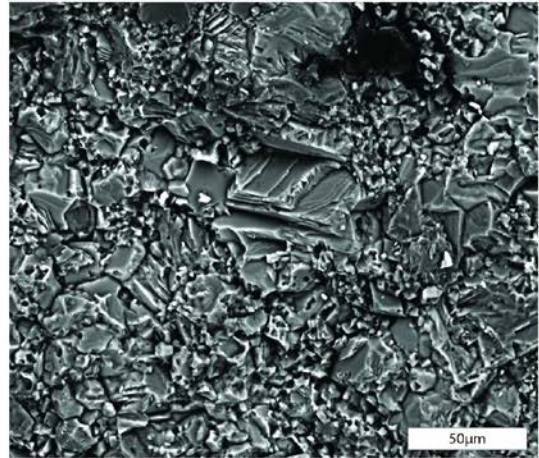


Figure 6. Detrital carbonate laminae from the Laney Member, JTM-BF-14, 133.4m depth. Minerals in this detrital layer are predominantly calcite and quartz with minor analcime. Quartz grains are sub-rounded to sub-angular, 15 to 60µm (silt size). Flattened carbonate clasts reach 110µm in length (sand size). Also shown are rounded fragments of organic matter. The matrix material is partly composed of compacted carbonate grains.

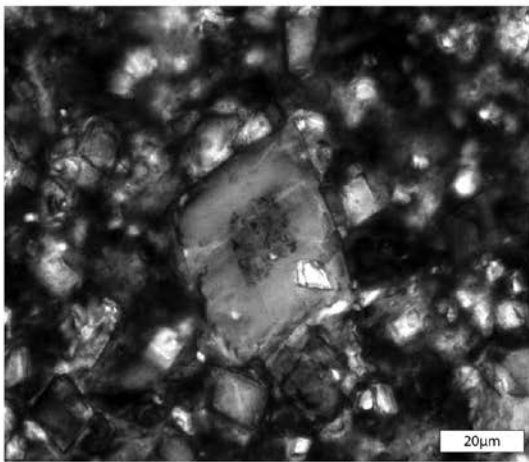
A



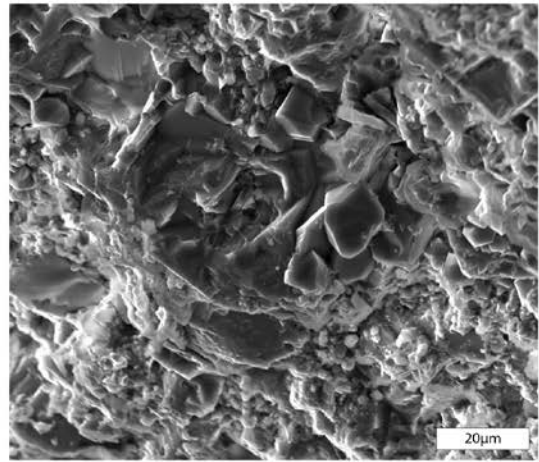
B



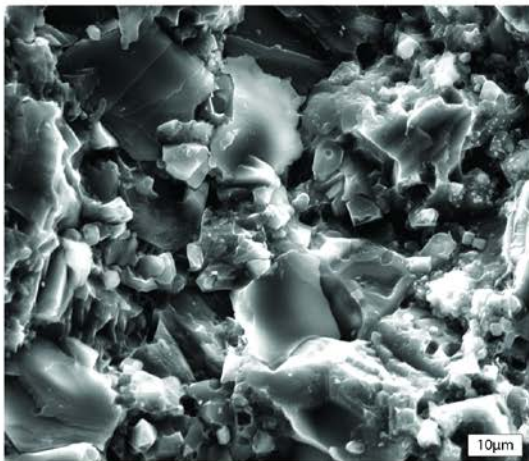
C



D



E



F

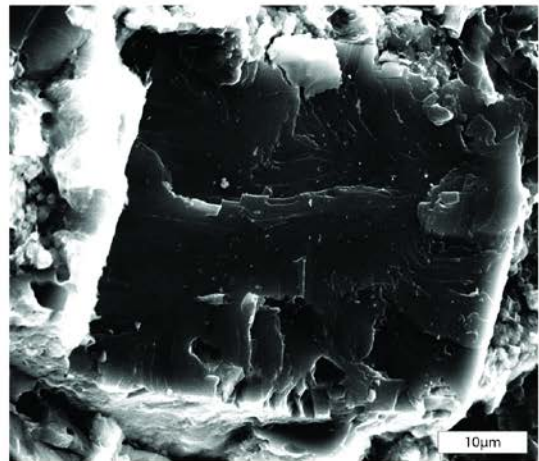


Figure 7. Hand sample (A), SEM (B, D, E, F) and thin section (C) images of carbonate crystals and textures observed in the Wilkins Peak Member. Sample A, B C, E, and F from JTM-BF-18 at 137.1m, and D from JTM-BF-19 at 138.2m. A) Dark laminae are predominantly dolomite mud made up of fine dolomite crystals ( $<15\mu\text{m}$  in diameter) and subhedral crystals of quartz. The lighter layers contain carbonate and quartz silt grains that are visible in hand sample. B) Backscatter SEM image displays the variable mineralogy and carbonate textures observed in the WPM. Crystal sizes in the sample range from  $<10\mu\text{m}$  to  $\sim 70\mu\text{m}$  in diameter and crystals are euhedral, subhedral, or anhedral. C) Thin section image of a dolomite rhomb with a cloudy core and clear margin. This suggests nucleation of dolomite overgrowth from a seed crystal. The cloudy nature of the core suggests a detrital origin. D) SEM image of dolomite overgrowths in a pure dolomite lamina. Crystals can grow to  $\sim 40\mu\text{m}$  in diameter and form well-developed faces. The majority of the crystals in this image are likely overgrowths on original seed crystals. E) SEM image of mixed calcite/dolomite layer showing variable crystal sizes typical of diagenetic dolomite. Dolomite rhombs form large well-developed crystals and calcite makes up the majority of the finer  $<10\mu\text{m}$  crystals. F) SEM image of large diagenetic dolomite rhombohedron  $>60\mu\text{m}$  in size.

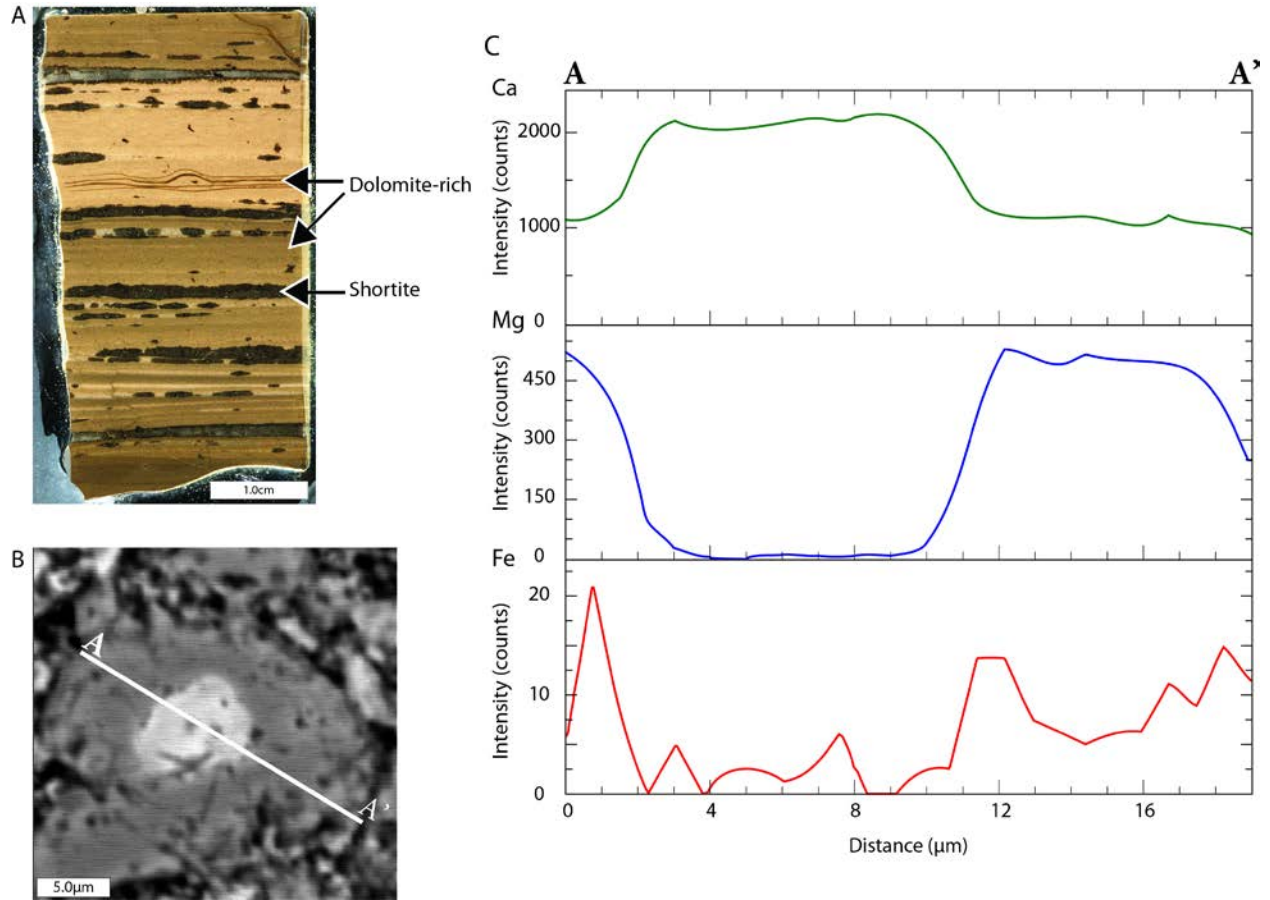


Figure 8. A) Alternating dolomite-rich laminae (light to dark brown depending on organic content) and diagenetic shortite (dark gray laminae, lenses, and pods) from JTM-BF-26, 154.0m. B) Electron microprobe backscatter image of a calcite grain with dolomite overgrowth from a dolomite-rich lamina in (A). C) Electron microprobe line scan through transect A-A'.

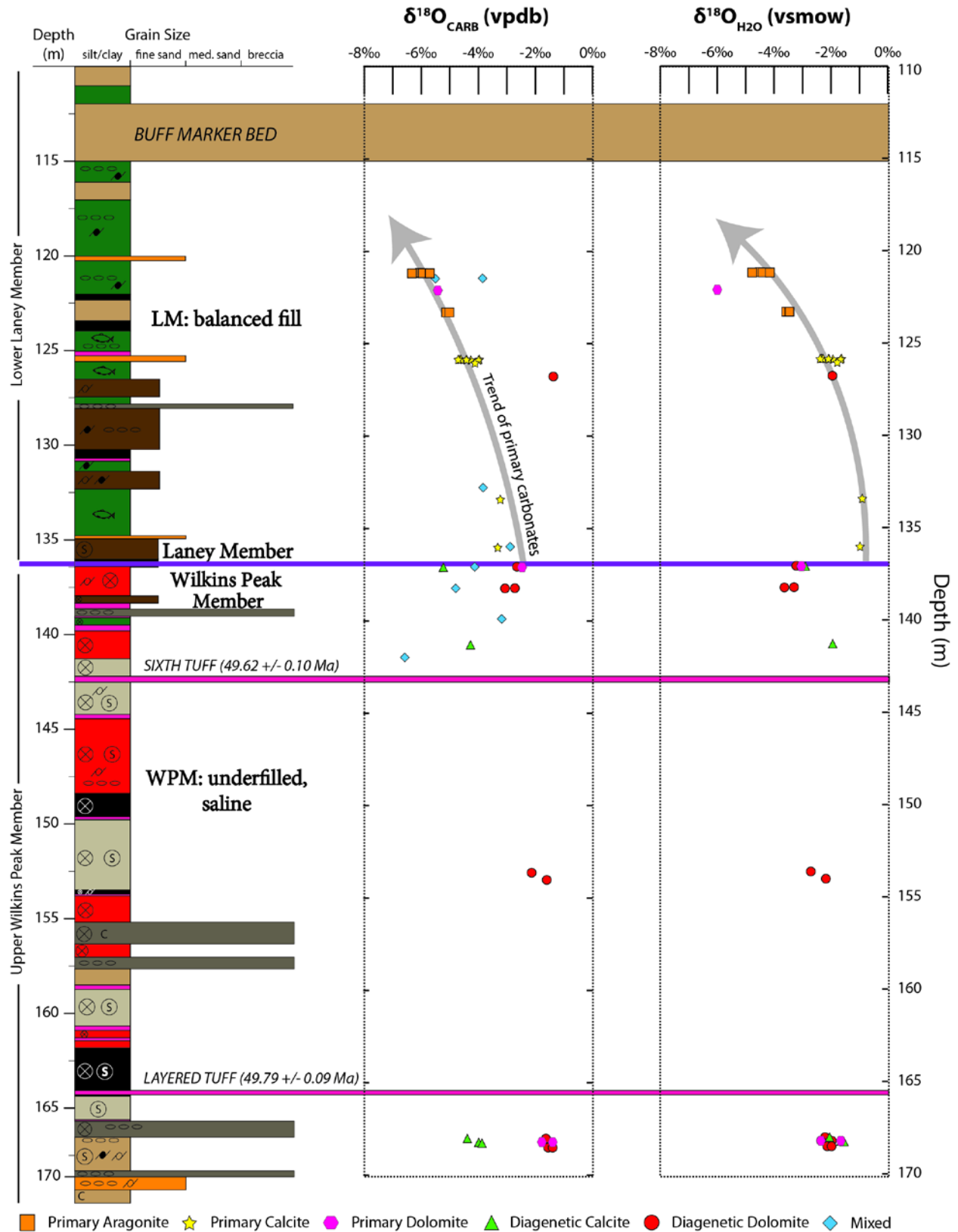
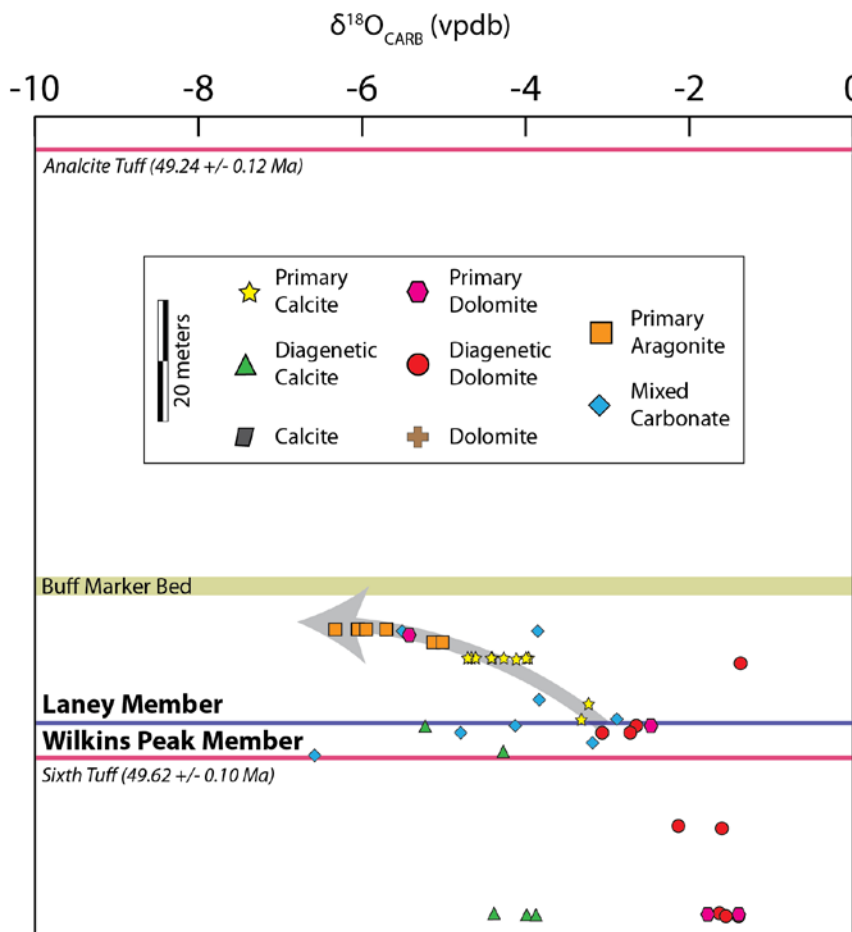


Figure 9. Stratigraphic section with  $\delta^{18}\text{O}_{\text{CARB}}$  and  $\delta^{18}\text{O}_{\text{H}_2\text{O}}$  isotopic data from the ERDA 1 Blacks Fork Core, Bridger Basin (See Figure 1 for location and Figure 2 for stratigraphic legend). No discernible isotopic trends were identified from the WPM. However, a systematic decrease in both  $\delta^{18}\text{O}_{\text{CARB}}$  and  $\delta^{18}\text{O}_{\text{H}_2\text{O}}$  is recorded by primary carbonates in the lower 15m of the Laney Member.

### ERDA 1 Blacks Fork Core - Bridger Basin This Study



### Arco Oil & Gas WB #1 Core - Washakie Basin Carroll et al. (2008); Doebbert et al. (2010); Chetel and Carroll (2010)

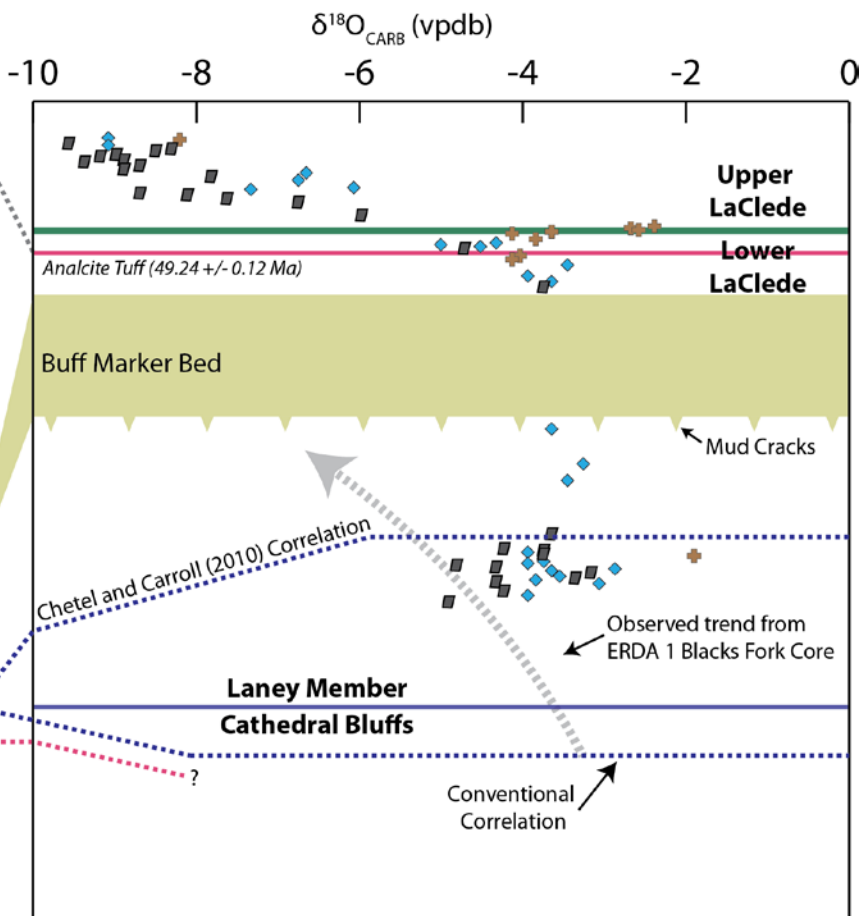


Figure 10. Comparison of isotopic data from the Wilkins Peak-Laney Member transitional zone (this study), with isotopic data from Carroll et al. (2008) for the Arco Oil & Gas WB #1 core, Washakie Basin, WY (see location on Figure 1). Data from the Bridger Basin are reported relative to the LM/WPM boundary and from the Laney Member/Cathedral Bluffs boundary in the Washakie Basin. Correlations across the basins are from Chetel and Carroll (2010). The 3-4 ‰ shift in primary carbonates observed in this study was not identified in the Washakie Basin, perhaps because of the bulk sampling used in Carroll et al. (2008).

Table 1. Minerals identified by X-ray powder diffraction from the Wilkins Peak and Laney Members, ERDA 1 Blacks Fork Core, Bridger Basin, Wyoming.

<i>Mineral</i>	<i>Formula</i>	<i>Member</i>
<i>Divalent Carbonates</i>		
Aragonite	CaCO <sub>3</sub>	LM
Calcite	CaCO <sub>3</sub>	WPM/LM
Dolomite	(CaMg)(CO <sub>3</sub> ) <sub>2</sub>	WPM/LM
<i>Framework Silicates</i>		
Quartz	SiO <sub>2</sub>	WPM/LM
Alkali Feldspars	K <sub>x</sub> Na <sub>1-x</sub> AlSi <sub>3</sub> O <sub>8</sub>	WPM/LM
Buddingtonite	NH <sub>4</sub> AlSi <sub>3</sub> O <sub>8</sub>	LM
Analcime	NaAlSi <sub>2</sub> O <sub>6</sub> ·H <sub>2</sub> O	LM
<i>Sodium Carbonates</i>		
Dawsonite	NaAlCO <sub>3</sub> (OH) <sub>2</sub>	WPM/LM
Shortite	Na <sub>2</sub> Ca <sub>2</sub> (CO <sub>3</sub> ) <sub>3</sub>	WPM
<i>Sulfides</i>		
Pyrite	FeS <sub>2</sub>	WPM/LM
<i>Rare or Trace Minerals</i>		
Gaylussite	Na <sub>2</sub> Ca(CO <sub>3</sub> ) <sub>2</sub> ·5H <sub>2</sub> O	WPM
Fluorite	CaF <sub>2</sub>	LM

Table 2. Sample name, depth, mineralogy, and stable isotope results of select laminae from the WPM-LM transition zone in the ERDA 1 Blacks Fork core. Bold rows indicate primary carbonate precipitates.

<i>Member</i>	<i>Sample #</i>	<i>Depth (m)</i>	<i>Total Mineralogy (%)</i>	$\delta^{18}\text{O}_{\text{CARB}}$ (vpdb) (‰)	$\delta^{18}\text{O}_{\text{H}_2\text{O}}$ (vsmow) (‰)
	<b>BF-2-L1</b>	<b>121.2</b>	<b>Aragonite (100)</b>	<b>-6.05</b>	<b>-4.50</b>
	<b>BF-2-L2</b>	<b>121.2</b>	<b>Aragonite (98); Quartz (2)</b>	<b>-6.05</b>	<b>-4.49</b>
	<b>BF-2-L3</b>	<b>121.2</b>	<b>Aragonite (100)</b>	<b>-5.70</b>	<b>-4.15</b>
	<b>BF-2-L4</b>	<b>121.2</b>	<b>Aragonite (92); Quartz (8)</b>	<b>-5.95</b>	<b>-4.40</b>
	<b>BF-2-L7</b>	<b>121.2</b>	<b>Aragonite (100)</b>	<b>-6.33</b>	<b>-4.77</b>
	<b>BF-2-L8</b>	<b>121.2</b>	<b>Aragonite (98); Quartz (2)</b>	<b>-5.71</b>	<b>-4.15</b>
	BF-3a	121.5	Sanidine (36); Aragonite (26); Dolomite (18); Quartz (12); Calcite (8)	-3.85	-
	BF-3c	121.5	Calcite (54); Dolomite (16); Sanidine (16); Quartz (14)	-5.51	-
	<b>BF-4e</b>	<b>122.1</b>	<b>Dolomite (77); Dawsonite (19); Quartz (4)</b>	<b>-5.42</b>	<b>-6.00</b>
	<b>BF-5a</b>	<b>123.3</b>	<b>Aragonite (77); Quartz (13); Analcime (10)</b>	<b>-5.13</b>	<b>-3.57</b>
	<b>BF-5b</b>	<b>123.3</b>	<b>Aragonite (79); Quartz (21)</b>	<b>-5.02</b>	<b>-3.46</b>
<b>Laney Member</b>	<b>BF-8a</b>	<b>125.8</b>	<b>Calcite (95.630); Quartz (4.3704)</b>	<b>-4.66</b>	<b>-2.33</b>
	<b>BF-8b</b>	<b>125.8</b>	<b>Calcite (94.294); Quartz (5.706)</b>	<b>-3.97</b>	<b>-1.63</b>
	<b>BF-8f</b>	<b>125.8</b>	<b>Calcite (86); Dolomite (12); Quartz (2)</b>	<b>-4.27</b>	<b>-1.93</b>
	<b>BF-8h</b>	<b>125.8</b>	<b>Calcite (87.240); Quartz (12.760)</b>	<b>-4.41</b>	<b>-2.07</b>
	<b>BF-8i</b>	<b>125.8</b>	<b>Calcite (95); Dolomite (3); Quartz (2)</b>	<b>-4.61</b>	<b>-2.28</b>
	<b>BF-8j</b>	<b>125.8</b>	<b>Calcite (88); Dolomite (10); Quartz (2)</b>	<b>-4.71</b>	<b>-2.38</b>
	<b>BF-8k</b>	<b>125.8</b>	<b>Calcite (97); Quartz (3)</b>	<b>-4.42</b>	<b>-2.09</b>
	<b>BF-8l</b>	<b>125.8</b>	<b>Calcite (84); Dolomite (13); Quartz (3)</b>	<b>-4.00</b>	<b>-1.66</b>
	BF-9a	126.0	Calcite (76); Dolomite (12); Analcime (6); Quartz (4); Pyrite (2)	-4.12	-1.78
	BF-10a	126.8	Dolomite (50); Buddingtonite (45); Quartz (5)	-1.37	-1.95
	BF-13g	132.8	Calcite (49); Quartz (19); Analcime (18); Dolomite (14)	-3.84	-
<b>BF-14b</b>	<b>133.4</b>	<b>Calcite (72); Analcime (22); Quartz (6)</b>	<b>-3.23</b>	<b>-0.90</b>	
BF-17a	136.0	Calcite (58); Dolomite (40); Quartz (2)	-2.89	-	
<b>BF-17c</b>	<b>136.0</b>	<b>Calcite (95); Quartz (5)</b>	<b>-3.32</b>	<b>-0.98</b>	
	BF-18a	137.1	Dolomite (73); Quartz (24); Dawsonite (3)	-2.65	-3.22
	BF-18b	137.1	Calcite (53); Dolomite (36); Quartz (11)	-4.13	-
	BF-18c	137.1	Calcite (94); Quartz (6)	-5.23	-2.90
<b>Wilkins Peak Member</b>	<b>BF-18d</b>	<b>137.1</b>	<b>Dolomite (87); Quartz (11); Dawsonite (2)</b>	<b>-2.47</b>	<b>-3.05</b>
	BF-19b	138.2	Dolomite (37); Quartz (34); Calcite (21); Analcime (8)	-4.80	-
	BF-19c	138.2	Dolomite (84); Albite (10); Quartz (6)	-3.07	-3.64

<b>BF-19d</b>	<b>138.2</b>	<b>Dolomite (87); Quartz (13)</b>	<b>-2.72</b>	<b>-3.30</b>
BF-20b	139.9	Calcite (39); Dolomite (38); Quartz (16); Shortite (7)	-3.18	-
BF-21b	141.3	Calcite (89); Quartz (11)	-4.27	-1.94
BF-22a	142.0	Orthoclase (38); Calcite (33); Gaylussite (20); Quartz (9)	-6.58	-
BF-25c	153.6	Dolomite (79); Calcite (13); Quartz (8)	-2.13	-2.71
BF-26a	154.0	Dolomite (76); Quartz (24)	-1.60	-2.18
BF-33b	168.0	Calcite (55); Sanidine (27); Dolomite (13); Quartz (5)	-4.39	-2.05
BF-33c	168.0	Dolomite (52); Sanidine (40); Quartz (8)	-1.63	-2.21
<b>BF-34a</b>	<b>168.2</b>	<b>Dolomite (84); Calcite (10); Quartz (6)</b>	<b>-1.78</b>	<b>-2.35</b>
BF-34b	168.2	Calcite (83); Dolomite (11); Quartz (7)	-2.08	-1.65
BF-34c	168.2	Calcite (76); Dolomite (15); Quartz (9)	-3.87	-1.54
<b>BF-34d</b>	<b>168.2</b>	<b>Dolomite (76); Microcline (20); Quartz (4)</b>	<b>-1.40</b>	<b>-1.98</b>
BF-35b	168.5	Dolomite (61); Anorthoclase (34); Quartz (5)	-1.55	-2.13
BF-35c	168.5	Dolomite (93); Quartz (8)	-1.40	-1.98

Table 3. Average Mg-content of select calcite crystals from the LM and WPM. Values were obtained from electron microprobe analysis.

Sample #	# of Samples	Mg-Content (average % MgCO <sub>3</sub> )
BF-8a	4	1.09
BF-8j	5	0.78
BF-17a	5	0.67
BF-17c	6	0.39
BF-18b	5	0.23
BF-34b	8	0.22
BF-34c	5	0.21

Table 4. Electron microprobe results from dolomite crystals which varied in iron concentration between the core and rim.

Sample ID	Depth (m)	% FeCO <sub>3</sub> (Core)	% FeCO <sub>3</sub> (Rim)
BF-18a	137.1	2.51	3.59
BF-18a	137.1	0.10	0.87
BF-18b	137.1	0.00	1.14
BF-18b	137.1	0.00	0.81
BF-18c	137.1	0.24	0.52
BF-18c	137.1	0.00	0.25
BF-26a	154.0	0.09	0.65